

Comparative investigation of concentrated photovoltaic thermal-thermoelectric with nanofluid cooling

The corrections made in this section will be reviewed and approved by a journal production editor.

Oussama Rejeb^{a,*} oussama.r009@hotmail.fr, Samson Shittu^b, Guiqiang Li^{b,*} Guiqiang.Li@hull.ac.uk, Chaouki Ghenaoui^{c,a,e}, Xudong Zhao^b, Christophe Ménézo^d, Abdelmajid Jemni^e, Mohamed hedi Jomaa^f, Maamar Bettayeb^{g,h}

^aSustainable Energy Development Research Group, Research Institute for Science and Engineering (RISE), University of Sharjah, P.O. Box 27272, Sharjah, United Arab Emirates
^aSustainable Energy Development Research Group, Sustainable Energy and Power Systems Research Center. Research Institute for Science and Engineering (RISE), University of Sharjah, P.O. Box 27272, Sharjah, United Arab Emirates

^bCentre for Sustainable Energy Technologies, University of Hull, HU6 7RX, UK

^cDepartment of Sustainable and Renewable Energy Engineering, College of Engineering, University of Sharjah, Sharjah, United Arab Emirates
^cDepartment of Sustainable and Renewable Energy Engineering, College of Engineering, University of Sharjah, Sharjah, United Arab Emirates.

^dUniversity Savoie Mont-Blanc, LOCIÉ UMR CNRS 5271, EUR Solar Academy- INES Campus Scientifique Savoie Technolac, F-73376 Le Bourget-du-Lac, France

^eUniversité de Monastir, Ecole Nationale d'Ingénieurs de Monastir (ENIM), Laboratoire d'Etudes des Systèmes Thermiques et Energétiques (LESTE), LR99ES31, 5000 Monastir, Tunisia

^fSchool of Electronics, Electrical Engineering and Computer Science, Queen's Advanced Micro-Engineering Centre, Queen's University Belfast, Ireland

^gDepartment of Electrical Engineering, University of Sharjah, Sharjah, United Arab Emirates

^hCenter of Excellence in Intelligent Engineering Systems (CEIES), King Abdulaziz University, Jeddah, Saudi Arabia

*Corresponding authors.

Abstract

Thermoelectric modules are capable of converting heat into electric energy via the Seebeck effect. Therefore the addition of the thermoelectric generator modules (TEG) between the PV module and the absorber plate inside a concentrated photovoltaic thermal (CPVT) solar collector can be a feasible way for to enhance their electrical generation. A comparison between the CPVT only system and CPVT system integrated with TEG (CPVT-TE) is conducted using numerical simulation. Therefore CPVT-TE with water and CPVT-TE with 0.5% graphene/water nanofluid is investigated. A transient study using the finite volume method is presented, and computation is performed for all the considered solar systems for a typical sunny day and cloudy day under London climatic conditions. The CPV and the outlet fluid temperatures, as well as, the energy and exergy calculations are carried out to assess the performance of all the considered solar systems. The results reveal that the improvements in the total electrical power generated by the CPVT-TE with 0.5% graphene/water nanofluid and CPVT-TE compared to CPVT collector are 11.15% and 9.787%, respectively for the summer day, while, that for the winter day is 5.14% and 4.528%, respectively. The reductions in the thermal power provided by the CPVT-TE with 0.5% graphene/water nanofluid and CPVT-TE compared to CPVT collector are 6% and 11.76%, for the summer day, while, that for the winter day are 10.534.86% and 4.8710.53%, respectively. Moreover, the total exergies generated by 0.5% graphene/water nanofluid CPVT-TE and water CPVT-TE collectors increased by 4.88% and 0.68% respectively, for the summer day, while that for the winter day are 3.252.99% and 0.95% respectively, in comparison with the conventional CPVT system.

Keywords: CPVT-TE; Energy; Exergy; Nanofluid; Thermal management

Nomenclature

A Area, m^2

C Optical concentration

C_p Specific heat capacity, $J/kg/K$

D Diameter, m

h heat transfer coefficient (W/m^2K)

I_{TE} current

l length (m)

m Mass (Kg)

N_{TE} Number of TEGs

n Number of the pairs

Nu Nusselt number

P_{TE} Electrical power provided by TEG, W/m^2

Pr Prandtl number

Q_{elec} Electrical power generated by CPV, m^2

Re Reynold's number

Nu Nusselt number

R heat resistance

R_{in} Internal load resistance

R_{load} External load resistance

T Temperature (K)

Greek symbols

α	Solar absorption coefficient, Seebeck coefficient (V/K)
β	Temperature conversion coefficient, (1/K)
δ	Thickness (m)
η	Efficiency
ρ	Density, kg/m ³
ν	Kinematic viscosity (m ² /s)
ϵ	emissivity
τ	Solar transmission
σ	Stefan-Boltzmann's constant ($5.67 * 10^{-8} Wm^{-2}K^{-4}$), thermoelectric materials resistivity (Ωm)

Subscripts

ad	adhesive
amb	ambient
c	Cold side of TE module
Conv	convective
Cu	Cu electrode
EVA	ethylene vinyl acetate
exer	exergy
g	glazing
h	Hot side of TE module
is	insulation
n	n-type element of TE module
p	p-type element of TE module
sc	Solar cells
tub	tubes
TE	Thermoelectric module
wf	Working fluid
sky	sky

1 Introduction

Research and development of clean and sustainable energy technologies have gained more attention recently due to the augmenting effect of environmental protection [1,2]. Solar energy is a clean, reliable, free and inexhaustible energy source, which offers a promising solution to reduce carbon fuel consumption and improve environmental issues [3,4]. Solar PV is one of the best promising technologies which has attracted significant interest in recent years due to its huge potential [5,6]. PV module converts solar radiation directly into electrical power with zero pollutant emission [7]. However, a PV module converts a small part of the absorbed solar radiation into electrical power and the rest is reflected to the atmosphere or absorbed as heat which increases the photovoltaic operating temperature [8,9]. The conversion efficiency of PV decreases as its temperature increases. In addition, dust accumulation, increased PV temperature and low conversion efficiency are the main barriers to the widespread application of PV [10]. Consequently, the photovoltaic conversion efficiency and life span can be increased by effective cooling and utilization of its waste heat [11,13][11-13].

The combination of PV and TE enables the utilization of a larger solar spectrum because the photovoltaic utilizes the visible and ultra-violet parts of the solar spectrum whereas the thermoelectric uses the infrared part [14]. Furthermore, a TE generator is a viable clean energy technology capable of generating electricity directly from waste heat via the Seebeck effect [15–19]. Thermoelectric generators are small size, reliable energy converts that provide zero noise due to the absence of moving mechanical parts and they cause no damage to the environment because of zero pollution [20]. However, just like the limitation of the photovoltaic, the thermoelectric generator also suffers from low conversion efficiency and high material cost which have hindered their wide spread applications [21–22]. Consequently, researchers have paid attention to integrating thermoelectric generators with photovoltaic as a strategy to obtain an increased overall efficiency due to the complimentary performance of both technologies. The two main integration methods for a hybrid photovoltaic-thermoelectric are: direct coupling and spectrum splitting methods. Using the direct coupling method, Li et al. [23] investigated the conflicting behaviour of the external load resistance attached to the thermoelectric in a TE only and hybrid PV-TE system. They noticed that maximum power output can be obtained from the thermoelectric only, thermoelectric in photovoltaic-thermoelectric and photovoltaic-thermoelectric at different external load resistance.

A concentrated photovoltaic (CPV) system concentrates incoming solar radiation onto a smaller photovoltaic cell using inexpensive optical devices such as lenses or mirrors [22,23]. Rezanian et al. [24] conducted performance evaluation of a concentrated photovoltaic-thermoelectric system. Results showed that active cooling of the TEG in the CPV-TE improved its efficiency. Lamba et al. [25] presented a numerical model for a CPV-TE hybrid. Results indicated that the CPV-TE obtained an enhanced efficiency and power output of 5% compared to those of the CPV module. Furthermore, Mahmoudinezhad et al. [26,27] presented two important studies on the behaviour of CPV-TE system under variable weather conditions. In [26], a one-dimensional thermally coupled model solved by finite volume method (FVM) was used and they found that the thermal contact resistance has a substantial impact on the electrical performance of the hybrid system. In addition to the experimental study carried out in [27], a 3D three dimensional numerical model was utilized to investigate the power output of hybrid system and they noticed that using a TEG stabilized the CPV-TE power output.

A consequence of high solar concentrations on the photovoltaic is the dramatic decrease in the PV efficiency due to increased temperature [28]. Therefore, the use of effective cooling systems in CPV is very important. Heat pipes can be used to transport heat over long distances using a small temperature difference [29]. Shittu et al. [30] presented a detailed three-dimensional comparative investigation on the efficiency of a CPV-TE with and without flat plate heat pipe. They noticed that the hybrid system with heat pipe is beneficial for high solar concentration application. Li et al. [31] presented a preliminary experimental work on a PV-TE coupled with micro-channel heat pipe. Results showed that the new hybrid system which also incorporated the heat pipe offered better electrical generated power in comparison to the conventional PV ones.

Phase change material (PCM) has been incorporated in the hybrid photovoltaic-thermoelectric for performance enhancement. A novel study on CPV-TE with PCM placed between the photovoltaic and thermoelectric generator was presented by Cui et al. [32]. They found that the negative influence of solar radiation variation in the CPV-TE was reduced by the use of phase change material. Furthermore, Motiei et al. [33] presented a two-dimensional transient study of a photovoltaic-thermoelectric hybrid system

with phase change material as the heat sink. The superior performance of the PV-TE system with PCM in comparison to that without PCM was observed. Likewise, Darkwa et al. [34] performed a theoretical and experimental study on a PV-TE system with PCM heat sink. They found that the PV temperature could be lowered effectively for a longer period by the use of thick PCM layer.

Yin et al. [35–37] presented the suitability of water-cooling for performance enhancement of a hybrid photovoltaic-thermoelectric. In [35], various methods for cooling the TEG were compared and results showed that water cooling provides the best hybrid system performance compared to air cooling. Furthermore, in [36], over a one-day period, the hybrid system performance was evaluated, and they found that cooling water mass significantly affects the hybrid system performance. In [37], an experimental study was performed to optimize the concentrated photovoltaic-thermoelectric with water cooling. Results showed that the optimized CPV-TE had a power output of 1.50 W which was higher than that of the CPV only system (1.38 W). Furthermore, Zhang and Xuan [38] studied the effectiveness of adjustable cooling water block in reducing the temperature fluctuation caused by variable solar radiation on the hybrid system performance. Experimental results showed negligible difference between the output power of the new system and that of PV-PCM-TE.

Nanofluids as cooling fluids in the PVT-TE collectors are important to improve heat transfer properties compared to conventional fluids [39–45]. The influence of nanofluid use in hybrid PV-TE was performed by Wu et al. [39]. They found that using nanofluid enhances the system efficiency in comparison to the water cooling fluid. Furthermore, an experimental study on PV-TE with nanofluid was presented by Soltani et al. [40] and they found that SiO₂/water nanofluid enhanced power output and efficiency by 54.29% and 3.35%, respectively. Similarly, Lekbir et al. [41] presented an innovative nanofluid photovoltaic-thermoelectric collector. In this solar collector, the nanofluid was considered as a working fluid which was used to absorb the heat from the TEG backside, thereby enhancing the overall hybrid system performance. They found that using nanofluid coolant provides a better alternative to manage the hybrid system energy production in comparison to other cooling methods.

An experimental comparison study on water PV-TE and Co₃O₄/water nanofluid PV/TE collectors was conducted by Rajaei et al. [43]. Their results showed that using nanofluid as a cooling fluid improves the gradient of the temperature between the hot and cold side of the TE module compared to water, consequently improving the TE modules' electrical power.

Kolahan et al. [44] investigated a PVT-TEG using an aluminium-oxide/water (Al₂O₃/water) nanofluid as a working fluid. A mathematical model using a finite volume method (FVM) was established. The results indicated an enhancement in the global electrical efficiency by the range of (2.5%–4%) and reduced the payback period by 12% provided by the PVT-TE compared PVT collector. A comparative experimental investigation between the concentrated photovoltaic/thermoelectric generator (CPV/TEG), water-based concentrated photovoltaic/thermal-thermoelectric generator (WCPV/T-TEG) and the nanofluid-based concentrated photovoltaic/thermal-thermoelectric generator (NCPV/T-TEG) has been carried out by Lekbir et al. [45]. The results revealed that the total net electrical powers generated by the NCPV/T-TEG, WCPV/T-TEG and conventional CPVT collectors were 2.02 W, 1.84 W and 1.73 W, respectively.

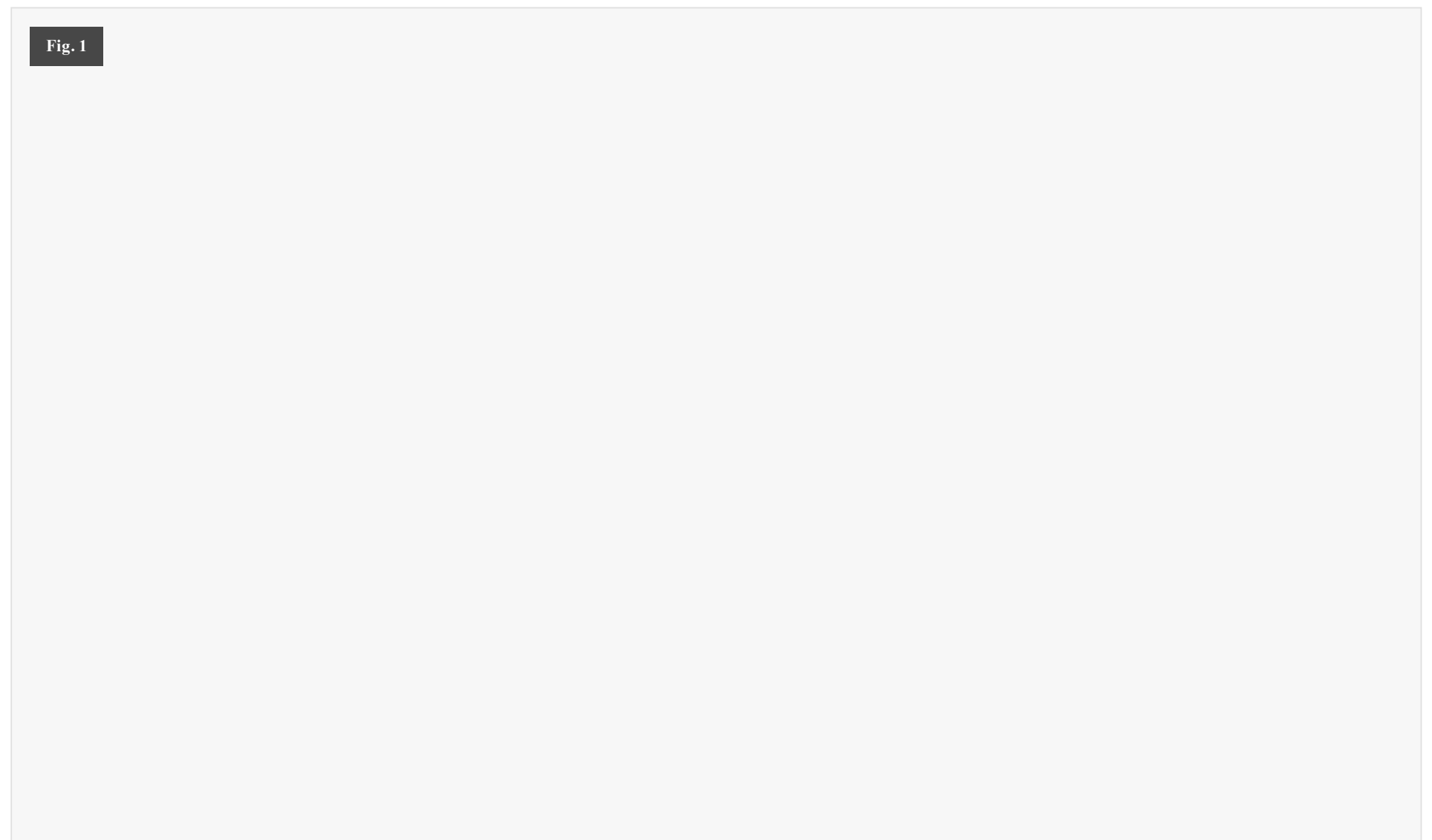
To our knowledge, no studies, investigating the behaviour of PV-TE using a nanofluid as a cooling fluid under temperate oceanic climate (cool winters and warm summers) have been published in the past, which indicates a substantial research gap. Moreover, few studies have been performed to investigate the impact of using different nanofluids as working cooling fluid, such as SiO₂-water and Fe₃O₄-water [42], Co₃O₄/water [43]. High thermal conductivity of graphene [46] exhibits the best improvement in the nanofluids' thermal characteristics. However, utilizing the graphene nanoplatelets-water nanofluid cooling in CPVT-TE collector is not available in the literature. Therefore, for the first time, this study presents a detailed comparison between the conventional CPVT, CPVT-TE with water and CPVT-TE with 0.5% graphene/water nanofluid from the temperature variation, energy and exergy viewpoints under London climatic condition

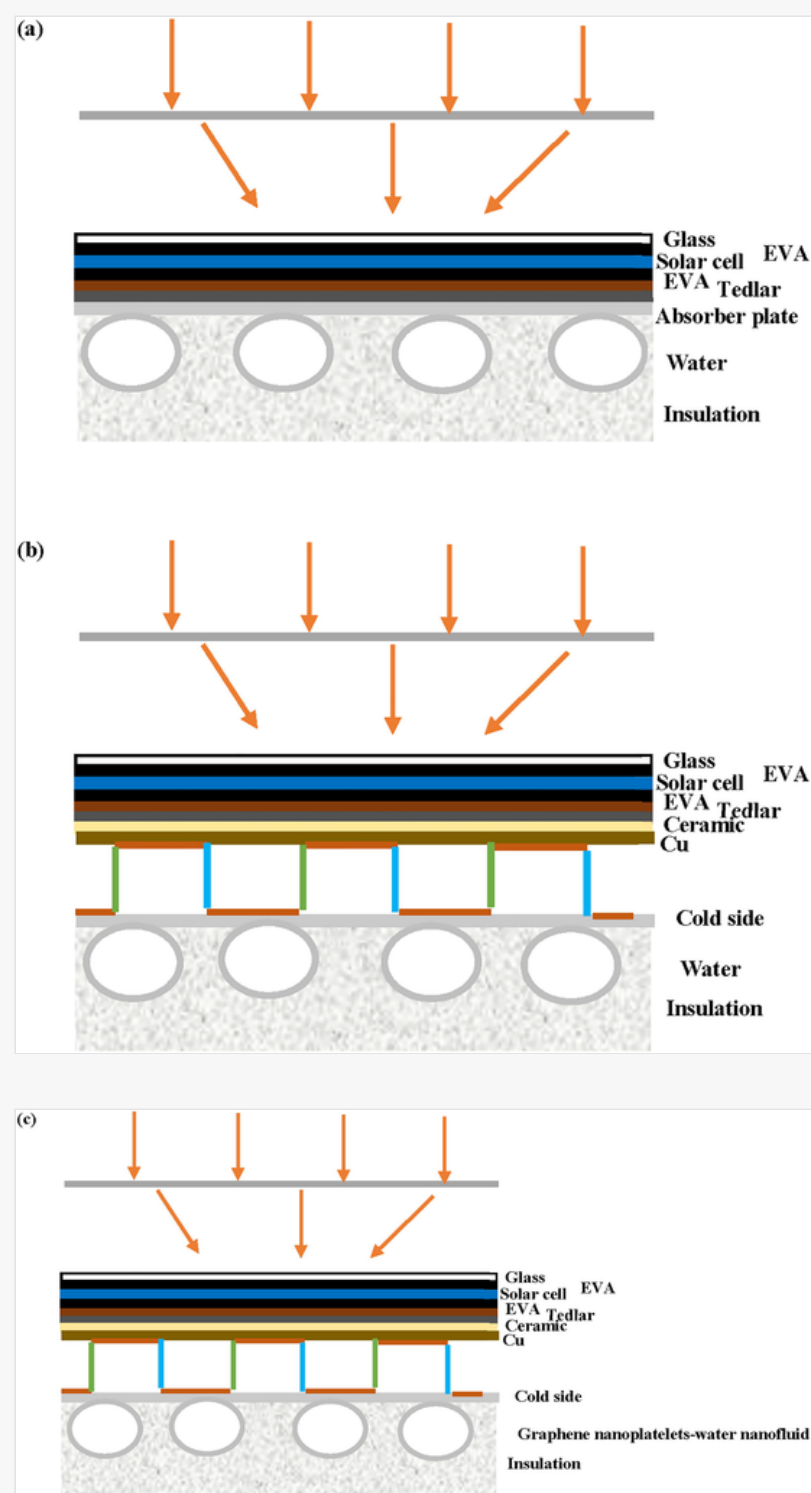
The paper is organized as follows: a physical description of the different considered systems (the conventional CPVT, CPVT-TE with water and CPVT-TE with 0.5% graphene/water nanofluid) is given in Section 2. The developed mathematical models for different considered systems are introduced in Section 3, including computation procedures and model validation. A comparison between all the considered solar systems from the temperature variation, energy and exergy viewpoints under London climatic condition is performed in Section 4, while the study's conclusion is presented in Section 5.

2 Hybrid system structure description

In this study, different systems are considered including one conventional concentrated photovoltaic thermal (CPVT) system and two different CPVT-TE hybrid systems using water and 0.5% graphene/water nanofluid as a cooling fluid (Fig. 1). The conventional CPVT (Fig. 1a) is used as a reference to analyse and compare the electrical and thermal performances of the proposed hybrid systems. The CPVT-TE system is made up of the solar concentrator, PV, TE modules and a cooling system. Table 1 shows the PV material properties considered in this study, Table 2 shows the other parameters used in the numerical simulation while Table 3 shows the temperature dependent thermoelectric material properties considered in this study.

Fig. 1





Schematic diagram of (a) conventional CPVT; hybrid CPVT-TE with (b) water cooling and (c) graphene nanoplatelets-water nanofluid cooling.

Table 1

i The table layout displayed in this section is not how it will appear in the final version. The representation below is solely purposed for providing corrections to the table. To preview the actual presentation of the table, please view the Proof.

PV material properties.

	Thickness (mm)	Thermal conductivity (W/(mK))	Reflectivity	Absorptivity	Transmissivity
Glass	3	1.8	0.04	0.04	0.92
EVA	0.5	148	0.02	0.08	0.9
Silicon	0.4	0.35	0.08	0.9	0.02
Tedlar	0.33	0.15	0.8	0.128	0.012
Gel (adhesive)	0.5	1.15	-	-	-

Table 2

i The table layout displayed in this section is not how it will appear in the final version. The representation below is solely purposed for providing corrections to the table. To preview the actual presentation of the table, please view the Proof.

Parameters utilised in the developed numerical code.

Area of the CPV	0.42 m²
Dimension of the thermoelectric module	40 mm × 40 mm × 3.8 mm
TE element number	127
Thickness of the Ceramic	0.8 mm
Thermal conductivity of the Ceramic	31 W/(mK)
Thickness of the Cu	0.3 mm
Thermal conductivity of the Cu	398 W/(mK)

Thermal conductivity of the insulation	0.045 W/(mK)
Density of the insulation	24 kg/m ³
Specific heat of the insulation	919 J/(kgK)

Table 3

i The table layout displayed in this section is not how it will appear in the final version. The representation below is solely purposed for providing corrections to the table. To preview the actual presentation of the table, please view the Proof.

The thermoelectric material properties [39].

Property	p-type polynomial equation	n-type polynomial equation
Seebeck coefficient (V/K)	$= -2.24407 * 10^{-11} T^3 + 2.22834 * 10^{-8} T^2 - 7.301 * 10^{-6} T + 1.023698 * 10^{-3}$ $= -2.24407 * 10^{-11} T^3 + 2.22834 * 10^{-8} T^2 - 7.301 * 10^{-6} T + 1.023698 * 10^{-3}$ (1)	$= 1.68178 * 10^{-11} T^3 - 1.77136 * 10^{-8} T^2 + 6.203 * 10^{-6} T + 9.54589 * 10^{-4}$ $= 1.68178 * 10^{-11} T^3 - 1.77136 * 10^{-8} T^2 + 6.203 * 10^{-6} T - 9.54589 * 10^{-4}$ (4)
Thermal conductivity (V/K)	$= -5.82609 * 10^{-8} T^3 + 1.03491 * 10^{-4} T^2 - 0.05011 T + 8.726$ (2)	$= 3.76869 * 10^{-9} T^3 + 2.81722 * 10^{-5} T^2 - 0.02057 * T + 5.09531$ (5)
Electrical resistivity (V/K)	$= -7.75456 * 10^{-13} T^3 + 7.77051 * 10^{-10} T^2 - 0.01853 * 10^{-5} T + 1.60117 * 10^{-5}$ (3)	$= -6.04782 * 10^{-13} T^3 + 6.09155 * 10^{-10} T^2 - 1.715 * 10^{-7} T + 2.11951 * 10^{-5}$ (6)

Solar concentrator is used in this study to increase the quantity of solar energy absorbed by the PV cell. The five layers that make up the photovoltaic module are: glass, ethylene vinyl acetate (EVA), silicon cell, EVA and Tedlar back. Furthermore, the TE module consists of the ceramic layers, Cu electrode layers and semiconductor p-type and n-type thermoelectric legs. Different thermal management cooling systems are employed at the bottom of the thermoelectric including water cooling (Fig. 1b), and graphene nanoplatelets-water nanofluid cooling (Fig. 1c). A direct-coupling integration approach is used for the hybrid systems in which the thermoelectric is connected directly to the rear area of the CPV cell by an adhesive (gel). Consequently, the excess heat from the PV cell is conveyed via conduction to the TE module thereby resulting in a reduced of the PV temperature and additional electrical power generation from the TE module via Seebeck effect. The cold side of the TE module is cooled using different methods (water and graphene nanoplatelets-water nanofluid) while Bismuth telluride (Bi₂Te₃) thermoelectric module is used in this study with 127 thermocouples. A performance comparison is presented in subsequent sections.

3 Numerical model description

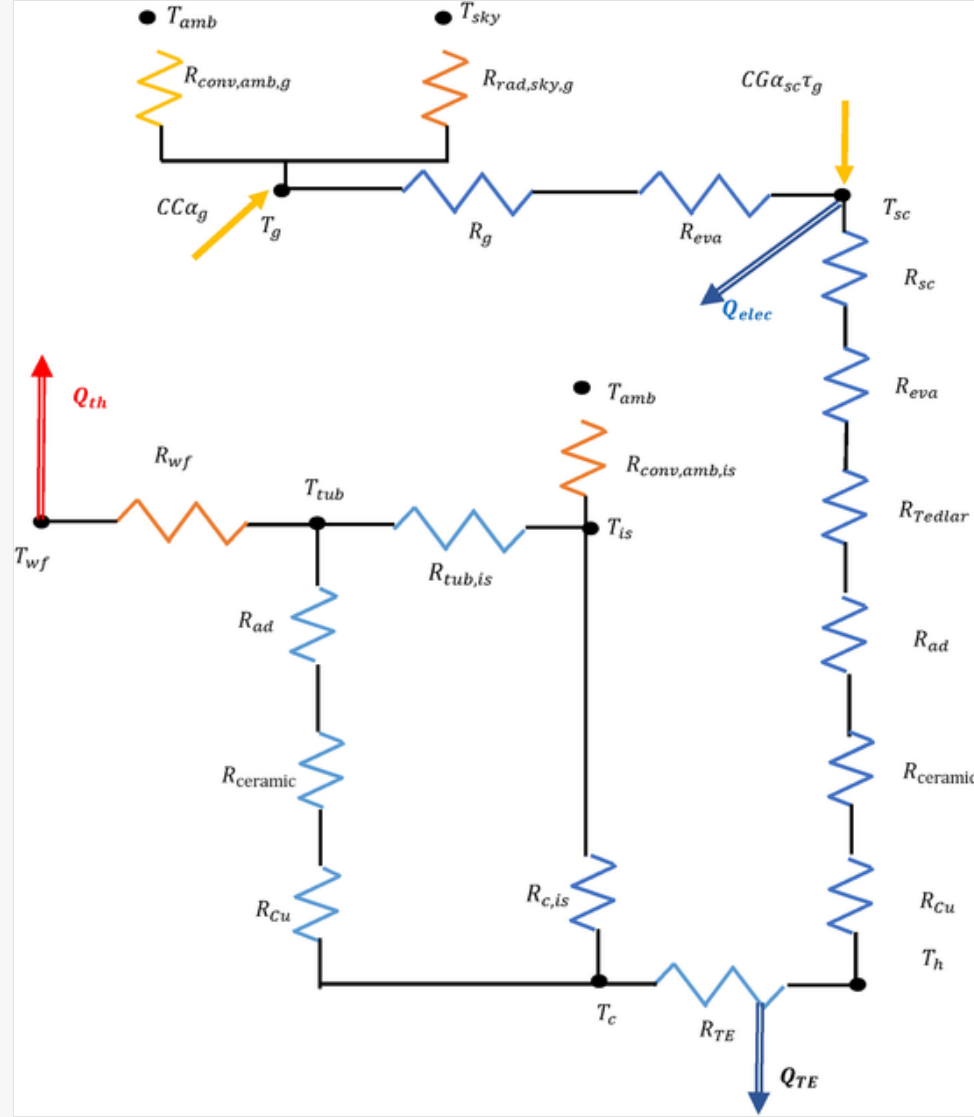
3.1 Mathematical model

To simply the model and facilitate the numerical simulation, the following hypotheses are considered:

- The properties of the PV module and the insulation are considered to be constant.
- The radiative heat loss from the backside collector is neglected.
- The working fluid mass flow rate is considered to be constant.
- Transient conditions are considered.

Based on the thermal resistance networks (Fig. 2), the energy balance of different components of the hybrid CPVT-TE is presented as follows:

Fig. 2



Schematic diagram of thermal resistance network of the hybrid CPV-TE.

The heat balance equation for the glazing is expressed as:

$$m_g C_g \frac{dT_g}{dt} = \alpha_g CG A_g + \frac{(T_{sky} - T_g)}{R_{rad,sky,g}} + \frac{(T_{amb} - T_g)}{R_{conv,amb,g}} + \frac{(T_{sc} - T_g)}{R_g + R_{EVA}} + A_g k_g \delta_g \left(\frac{\partial^2 T_g(x,y)}{\partial x^2} + \frac{\partial^2 T_g(x,y)}{\partial y^2} \right) \quad (7)$$

where m_g , A_g , C_g , k_g , τ_g and δ_g are the mass, area, the specific heat, thermal conductivity, transmissivity and thickness of the glazing, respectively. $R_{rad,s,g}$ and $R_{conv,amb,g}$ are the radiative and convective heat resistance from the glazing to the environment and from the PV module to the sky, respectively. T_{sc} is the temperature of CPV module; T_g is the temperature of the glazing; R_g and R_{EVA} are the conduction heat resistances of the glazing and the EVA, respectively.

The radiative heat resistance ($R_{rad,sky,g}$) between the collector and the surroundings is related to the Stefan–Boltzmann constant (σ), surface of the glazing (A_g), emissivity of glazing module (ϵ_g) and the sky (T_{sky}) and glazing (T_g) temperatures. The following expression can describe it.

$$R_{rad,sky,g} = \frac{1}{A_g \epsilon_g \sigma (T_{sky}^2 + T_g^2) (T_{sky} + T_g)} \quad (8)$$

The convective heat resistance ($R_{conv,amb,g}$) is related to the wind velocity (u_{wind}), and the area of the PV module. The following expression can describe it.

$$R_{conv,amb,g} = \frac{1}{A_g (2.8 + 3 * u_{wind})} \quad (9)$$

The heat balance equation for the solar cells in CPV module is expressed as:

$$m_{sc} C_{sc} \frac{dT_{sc}}{dt} = \alpha_{sc} \tau_g CG A_{pv} - Q_{elec} A_{sc} + \frac{(T_g - T_{sc})}{R_g + R_{EVA}} + \frac{(T_h - T_{sc})}{R_{sc} + R_{eva} + R_{tedlar} + R_{ad} + R_{ceramic} + R_{Cu}} + A_{sc} k_{sc} \delta_{sc} \left(\frac{\partial^2 T_{sc}(x,y)}{\partial x^2} + \frac{\partial^2 T_{sc}(x,y)}{\partial y^2} \right) \quad (10)$$

where m_{sc} , A_{sc} , C_{sc} , k_{sc} and δ_{sc} are the mass, area, the specific heat, thermal conductivity and thickness of the solar cells in CPV module, respectively. Q_{elec} is the solar cells electrical energy output. R_{sc} , R_{eva} , R_{tedlar} , R_{ad} , $R_{ceramic}$ and R_{Cu} are the conduction heat resistances of the solar cells, EVA resin, Tedlar, adhesive, ceramic and the Cu electrode; T_h is the temperature of the hot side of the TE module.

The heat balance equation for the TE hot side module is expressed as:

$$m_h C_h \frac{dT_h}{dt} = \frac{(T_{sc} - T_h)}{R_{sc} + R_{eva} + R_{tedlar} + R_{ad} + R_{ceramic} + R_{Cu}} + A_h k_h \delta_h \left(\frac{\partial^2 T_h(x,y)}{\partial x^2} + \frac{\partial^2 T_h(x,y)}{\partial y^2} \right) - (N_{TE} \alpha I_{TE} T_h) + (N_{TE} 0.5 I_{TE}^2 R_{in}) + (N_{TE} \frac{(T_c - T_h)}{R_{TE}}) \quad (11)$$

where m_h, C_{ph}, k_h and δ_h represent, the mass, the specific heat, thermal conductivity and the thickness of the hot side of TE module, respectively; I_{TE} is electrical current of the TE; R_{TE} is the semiconductor legs resistance. T_c is the temperature of the cold side of the TE module; R_{in} is the internal resistance; α is the Seebeck coefficient of TE.

The resistance of the semiconductor legs (R_{TE}) can be described by the following equation:

$$\frac{1}{R_{TE}} = n \left(\frac{k_n A_n}{l_n} + \frac{k_p A_p}{l_p} \right) \quad (12)$$

The internal resistance of TE is expressed by the following correlation

$$R_{in} = n \left(\frac{\sigma_n l_n}{A_n} + \frac{\sigma_p l_p}{A_p} \right) \quad (13)$$

where $k_n, \sigma_n, l_n, \sigma_n, A_n$ represent, the thermal conductivity, **electrical resistivity**, the length and the area of n-type element of TE module. $k_p, \sigma_p, l_p, \sigma_p, A_p$ represent, the thermal conductivity, **electrical resistivity**, the length and the area of p-type element of TE module.

The heat balance equation for the TE cold side module is expressed as:

$$m_c C_c \frac{dT_c}{dt} = \frac{(T_{tub} - T_c)}{R_{Cu} + R_{ad} + R_{ceramic}} + \frac{(T_c - T_{is})}{R_{c,is}} + A_c k_c \delta_c \left(\frac{\partial^2 T_h(x,y)}{\partial x^2} + \frac{\partial^2 T_h(x,y)}{\partial y^2} \right) + (N_{TE} \alpha I_{TE} T_c) + (N_{TE} 0.5 I_{TE}^2 R_{in}) + \left(N_{TE} \frac{(T_h - T_c)}{R_{TE}} \right) \quad (14)$$

where m_c, C_{pc}, k_c and δ_c represent, the mass, the specific heat, thermal conductivity and the thickness of the cold side of TE module, respectively. $R_{c,is}$ is the heat resistance by conduction between the cold side of TE module and the insulation. T_{tub} is the temperature of the tube.

The heat balance equation for the tube can be expressed as:

$$\frac{(T_c - T_{tub})}{R_{Cu} + R_{ad} + R_{ceramic}} + \frac{(T_f - T_{tub})}{R_{wf}} + \frac{(T_{is} - T_{tub})}{R_{tub,is}} = A_{tub} \rho_{tub} \delta_{tub} C_{tub} \frac{dT_{tub}}{dt} \quad (15)$$

where C_{tub}, ρ_{tub} and δ_{tub} represent, respectively, the density and the specific heat, density and the thickness of the tube. R_{wf} is the heat resistance by convection between the tube and the working fluid; $R_{tub,is}$ is the heat resistance by conduction between the tube and the insulation.

The heat balance equation for the cooling fluid can be expressed as:

Previous Version

$$\frac{(T_{tub} - T_{wf})}{R_{wf}} = A_{w,f} \rho_{w,f} C_{pw,f} \frac{dT_{w,f}}{dt} + \dot{m}_{w,f} C_{pw,f} \frac{dT_{w,f}}{dx} \quad (16)$$

Updated Version

$$\frac{(T_{tub} - T_{wf})}{R_{wf}} = A_{w,f} \rho_{w,f} C_{pw,f} \left(\frac{dT_{w,f}}{dt} + u_{wf} \frac{dT_{w,f}}{dy} \right)$$

where $\rho_{w,f}$ and $C_{pw,f}$ represent, respectively, the density and the specific heat of the cooling fluid. $\dot{m}_{w,f}$ and $u_{w,f}$ is the **mass fluid flow rate velocity**.

The convection transfer coefficient is related to the conductivity of cooling fluid, Nusselt number and the hydraulic diameter, given as

$$h_w = \frac{Nu_{cooling} K_{cooling}}{D_t} \quad (17)$$

To know the regime of flow occurring inside the tube (laminar, turbulent), the Reynold's number needs to be calculated. It is related to the fluid velocity inside the tube ($V_{cooling}$), hydraulic diameter (D_t) and the viscosity of water (θ).

$$Re = \frac{D_t V_{cooling}}{\theta} \quad (18)$$

For laminar flow, ($Re \leq 2300$), the convection transfer coefficient can be expressed as:

$$h_w = \frac{4.364K_{cooling}}{D_t} \quad (19)$$

For turbulent flow, ($Re > 2300$) the convection transfer coefficient can be expressed as:

$$h_w = \frac{(0.023Re^{0.8}Pr^{0.4})K_{cooling}}{D_t} \quad (20)$$

The thermophysical properties of the cooling fluids (water) as a function of the temperature are determined by the following equations:

Previous Version

$$\text{Density } \rho_w = -0.003T^2 + 1.505T + 816.781$$

Updated Version

Density :

$$\rho_w = -0.003T^2 + 1.505T + 816.781$$

(21)

Previous Version

$$\text{Specific heat } C\rho_w = -0.003T^2 + 1.505T + 816.781$$

Updated Version

Specific heat :

$$C\rho_w = -4.63 \cdot 10^{-5}T^3 + 0.0552T^2 - 20.86T + 6719.63$$

(22)

Previous Version

$$\text{Thermal conductivity } K_w = -0.000007T^2 + 0.0068T - 0.54$$

Updated Version

Thermal conductivity :

$$K_w = -7.843 \cdot 10^{-6}T^2 + 0.0062T - 0.54$$

(23)

Previous Version

$$\text{Viscosity } \mu_w = -0.00002414 * 10^{\frac{247.8}{7-140}}$$

Updated Version

Viscosity :

$$\mu_w = -2.414 \cdot 10^{-5} * 10^{\left(\frac{247.8}{7-140}\right)}$$

(24)

According to the principle of thermal equilibrium between the nanoparticles and the base fluid (water), the density, the specific heat the thermal conductivity and the viscosity of the nanofluid are determined by the following equations:

Density

$$\rho_{nf} = (1 - \varphi)\rho_{p,bf} + (\varphi)\rho_{p,np} \quad (25)$$

Specific heat

$$(C_p)_{nf} = (1 - \varphi)(C_p)_{p,bf} + (\varphi)(C_p)_{p,np} \quad (26)$$

Thermal conductivity

$$K_{nf} = \frac{[(K_{np} + 2K_{bf}) + 2\varphi(K_{np} - K_{bf})]}{[(K_{np} + 2K_{bf}) - \varphi(K_{np} - K_{bf})]} \quad (27)$$

Viscosity

$$\mu_{nf} = \frac{\mu_f}{(1 - \varphi)^{2.5}} \quad (28)$$

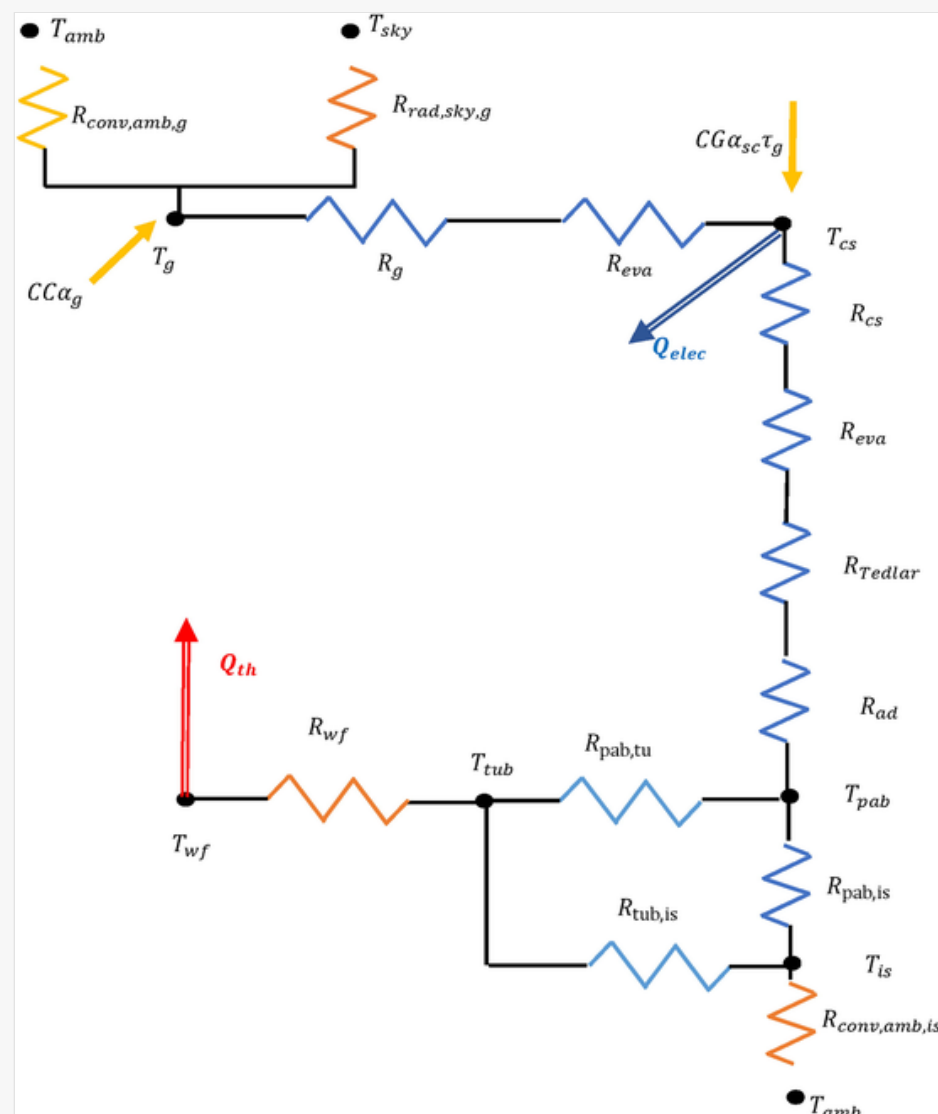
The heat balance equation for the insulation is given as:

$$m_{is}C_{is}\frac{dT_{is}}{dt} = \frac{(T_c - T_{is})}{R_{c,is}} + \frac{(T_{tub} - T_{is})}{R_{tub,is}} + \frac{(T_{amb} - T_{is})}{R_{conv,amb,is}} + A_{is}k_{is}\delta_{is}\left(\frac{\partial^2 T_{is}(x,y)}{\partial x^2} + \frac{\partial^2 T_{is}(x,y)}{\partial y^2}\right) \quad (29)$$

where m_{is} , $C_{p,is}$, k_{is} and δ_{is} are the mass, the specific heat, thermal conductivity and the thickness of the insulation, respectively.

Based on the thermal resistance networks (Fig. 3), the energy balance of different components of the hybrid CPVT is presented as follows:

Fig. 3



Schematic diagram of the conventional CPVT thermal resistance network.

The heat balance equation for the solar cells in CPV module is expressed as:

$$m_{sc} C_{sc} \frac{dT_{sc}}{dt} = \alpha_{sc} \tau_g CG A_{pv} - Q_{elec} A_{sc} + \frac{(T_g - T_{sc})}{R_g + R_{EVA}} + \frac{(T_{pab} - T_{sc})}{R_{cs} + R_{EVA} + R_{Tedlar} + R_{ad}} + A_{sc} k_{sc} \delta_{sc} \left(\frac{\partial^2 T_{sc}(x,y)}{\partial x^2} + \frac{\partial^2 T_{sc}(x,y)}{\partial y^2} \right) \quad (30)$$

The heat balance equation for the absorber plate is expressed as:

$$m_{pab} C_{pab} \frac{dT_{pab}}{dt} = \frac{(T_{sc} - T_{pab})}{R_{sc} + R_{EVA} + R_{Tedlar} + R_{ad}} + \frac{(T_{tub} - T_{pab})}{R_{pab,tu}} + \frac{(T_{is} - T_{pab})}{R_{c,is}} + A_{pab} k_{pab} \delta_{pab} \left(\frac{\partial^2 T_{pab}(x,y)}{\partial x^2} + \frac{\partial^2 T_{pab}(x,y)}{\partial y^2} \right) \quad (31)$$

The heat balance equation for the tube can be expressed as:

$$\frac{(T_{pab} - T_{tub})}{R_{pab,tu}} + \frac{(T_f - T_{tub})}{R_{wf}} + \frac{(T_{is} - T_{tub})}{R_{tub,is}} = A_{tub} \rho_{tub} \delta_{tub} C_{tub} \frac{dT_{tub}}{dt} \quad (32)$$

The heat balance equation for the insulation is given as:

$$m_{is} C_{is} \frac{dT_{is}}{dt} = \frac{(T_{pab} - T_{is})}{R_{c,is}} + \frac{(T_{tub} - T_{is})}{R_{tub,is}} + \frac{(T_{amb} - T_{is})}{R_{conv,amb,is}} + A_{is} k_{is} \delta_{is} \left(\frac{\partial^2 T_{is}(x,y)}{\partial x^2} + \frac{\partial^2 T_{is}(x,y)}{\partial y^2} \right) \quad (33)$$

3.2 Performance assessment

The electrical power (P_{TE}) provided by TEG is related to the output voltage (V_{out}) and the current (I_{TE}), and it given as:

$$P_{TE} = V_{out} I_{TE} \quad (34)$$

The current (I_{TE}) is related to the voltage source (V_{oc}), the external load resistance (R_{load}) and the internal load resistance (R_{in}), and it given as:

$$I_{TE} = \frac{V_{oc}}{R_{in} + R_{load}} \quad (35)$$

The following expression can determine the voltage source:

$$V_{oc} = \alpha \Delta T \quad (36)$$

The following expression can determine the Seebeck coefficient of TE

$$\alpha = n(\alpha_p - \alpha_n) \quad (37)$$

The following expression can determine the output voltage (V_{out}) [47]:

$$V_{out} = V_{oc} N_{TE} - I_{TE} R_{in} N_{TE} \quad (38)$$

Where N_{TE} is the number of TEGs.

The electrical power generated by the solar cells (Q_{elec}) is estimated applying the following correlation:

$$Q_{elec} = \alpha_{sc} \tau_g GC \eta_{elec} Pac \eta_0 [1 - \beta(T_{pv} - T_{ref})] \quad (39)$$

where $\hat{\eta}_{elec}$ represents the electrical efficiency at standard conditions ($T_{ref} = 298K$), β is the temperature conversion coefficient, and C is the optical concentration.

The thermal power of the solar hybrid collector is obtained from the expression below:

$$E_{th} = \dot{m}_w C_{pw} (T_{out} - T_{in}) \quad (40)$$

Exergy is defined as the available quantity of any potential energy and describes the qualitative aspect of the energy. Consequently, the exergy idea is considered as an important tool to evaluate systems; especially one the system possesses different kinds of energy sources

The thermal exergy power of the solar hybrid collector is obtained from the expression below:

$$\dot{E}_{\text{exer,th}} = E_{th} \left(1 - \frac{T_{\text{amb}}}{T_{\text{out}}} \right) \quad (41)$$

The total exergy power is determined by:

$$\dot{E}_{\text{exer,tot}} = \dot{E}_{\text{exer,th}} + \dot{E}_{\text{exer,elec}} + \dot{E}_{\text{exer,TE}} \quad (42)$$

where $\dot{E}_{\text{exer,elec}}$ and $\dot{E}_{\text{exer,TE}}$ are the electrical exergy power generated by CPV and BY TE modules, respectively

with

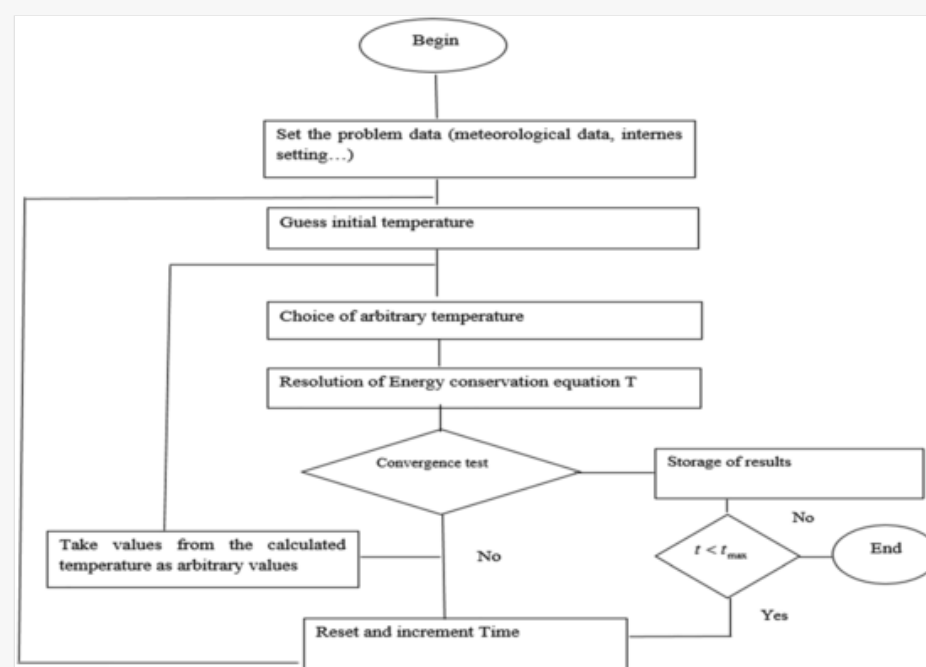
$$\dot{E}_{\text{exer,elec}} = E_{\text{elec}} \quad (43)$$

$$\dot{E}_{\text{exer,TE}} = P_{TE} \quad (44)$$

3.3 Computational procedure

The transient, two-dimensional modelling of the conventional CPVT and CPV-TE hybrid system with water and with graphene nanoplatelets-water nanofluid cooling fluid is developed in FORTRAN 90 using finite volume method. The flow chart of the calculation procedure is shown in Fig. 4.

Fig. 4

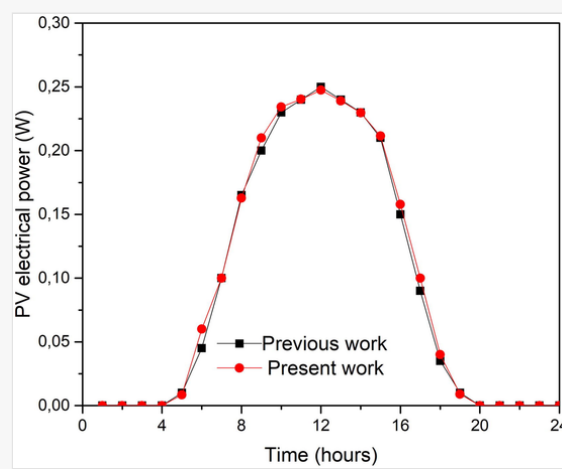


Flow chart of calculation procedure.

3.4 Model validation

Using results from previously published work by Motiei et al. [33], the numerical model utilized in this investigated is validated. In their study, a PV-TE system was simulated and results from that study are compared to the present study. Numerical conditions are reset to those in the referenced study [33] and the electrical power generated by the PV in the PV-TE hybrid system is shown in Fig. 5. As can be seen from this figure, the results performed from the previous investigation and the present work are very similar, and in good agreement therefore, the numerical model in this study is validated and accurate. Consequently, the results of this present work are reliable.

Fig. 5

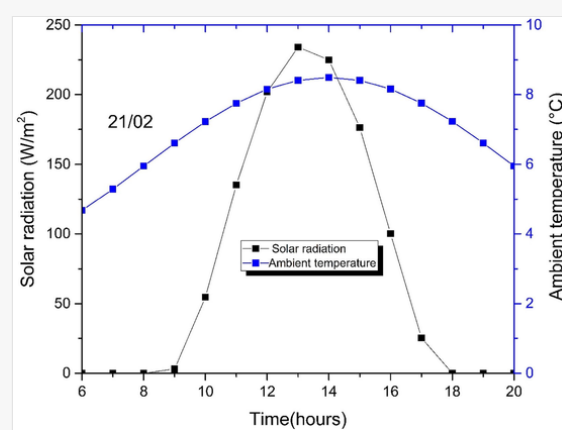


Model validation of the electrical power generated by the PV in the PV-TE hybrid system with [33].

4 Results and discussion

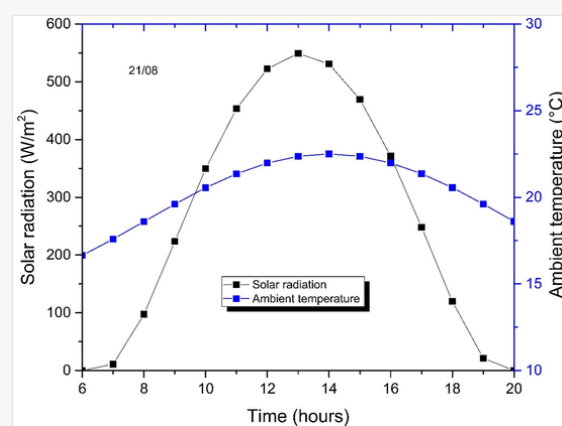
In this study, a typical sunny day and cloudy day under London climatic conditions ($51^{\circ}30'N$, $0^{\circ}7'E$) are considered and the weather data including the solar radiation and ambient temperature are shown in Figs. 6, and 7, respectively while the wind speed is fixed at 1 m/s. During the sunny day (21 August), the solar radiation fluctuates from 0 W/m^2 to 549 W/m^2 , and the ambient temperature changes from 16.7°C to 22.5°C . However, for the cloudy day (21 February), the solar radiation varies from 0 W/m^2 to 234 W/m^2 , and the ambient temperature ranges from 4.8°C to 8.4°C .

Fig. 6



Climatic conditions (solar radiation, ambient temperature) for cloudy day under London climatic conditions.

Fig. 7



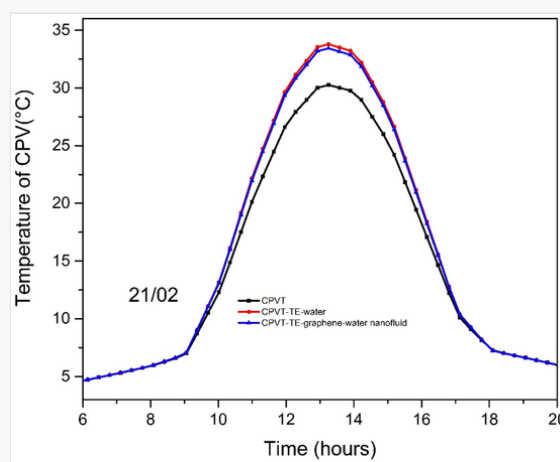
Climatic conditions (solar radiation, ambient temperature) for sunny day under London climatic conditions.

4.1 Temperature variation

4.1.1 CPV temperature

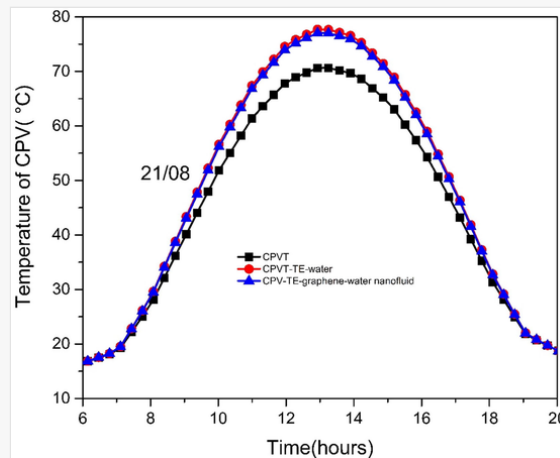
As shown in Fig. 8, for a cloudy day (21/02) under London climatic conditions, the CPV temperature of the conventional CPVT collector increases from 4.23°C to 30.32°C , while the CPV temperature of the CPVT-TE with water as cooling fluid and with 0.5% w.t graphene/water nanofluid increase from 4.64°C to 33.87°C , and from 4.64°C to 33.52°C respectively. Furthermore, as shown in Fig. 9, for a sunny day (02/08), the CPV temperature of the conventional CPVT collector increases from 16.5°C to 70.85°C , while the CPV temperature of the CPVT-TE with water as cooling fluid and with 0.5% w.t graphene /water nanofluid increase from 16.6°C to 77.96°C , and from 16.6°C to 77.29°C respectively.

Fig. 8



Variation of CPV for different considered system for cloudy day under London climatic conditions.

Fig. 9



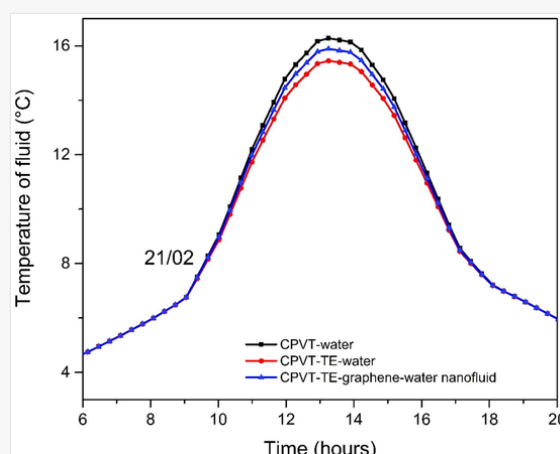
Variation of CPV for different considered system for sunny day under London climatic conditions.

This higher temperature of CPV in CPVT-TE compared to CPVT design is related to the thermal resistance of TE modules which minimises the cooling impact of the heat transfer fluids. On the other hand, adding the nanoparticles (graphene) in the base fluid (water) caused an enhancement in the convective heat transfer coefficient between the cooling fluid, and the tube wall due to the higher thermal conductivity of the graphene compared to the water. These phenomena contribute to the higher outlet 0.5% w.t graphene/water nanofluid temperature compared to conventional fluid (water). Due to the lower thermal conductivity of the TE module, the effect of cooling the CPV module using 0.5% w.t graphene /water nanofluid in CPVT-TE is negligible.

4.1.2 Outlet cooling fluid temperature

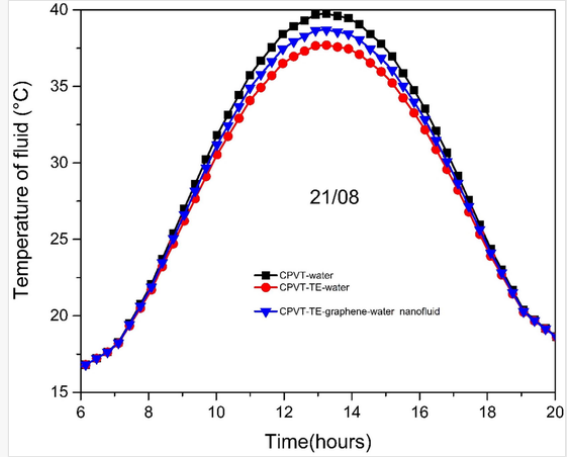
As seen in Figs. 10 and 11, the conventional CPVT collector has higher outlet fluid temperature compared to CPVT-TE with water and CPVT-TE with 0.5% graphene/water nanofluid. For a chosen summer day (21/08) in London region, which follows the oceanic climate temperature conditions, the fluid temperature of the CPVT collector increased from 16.6 °C to 39.8 °C, while the fluid temperature of CPVT-TE collector using water and using 0.5% graphene/water nanofluid increased from 16.6 °C to 37.76 °C and from 16.6 °C to 38.76 °C respectively. On the other hand, for a chosen winter day (21/02) in London region, the fluid temperature of the CPVT collector increased from 4.6 °C to 16.29 °C, while the fluid temperature of CPVT-TE collector using water and using 0.5% graphene/water nanofluid increased from 4.6 °C to 15.46 °C and from 4.6 °C to 15.91 °C respectively. For all the studied hybrid solar collectors, it is noted that the outlet fluid temperature in summer is higher compared to winter, which is due to the higher weather conditions in summer, i.e. ambient temperature and solar radiation. Furthermore, the CPVT results in higher outlet fluid temperature compared to the CPVT-TE collector using water and using 0.5% graphene/water nanofluid. In the CPVT-TE design, the heat loss by conduction from the solar cells to the absorber through the thermoelectric modules is higher than the heat loss from the solar cells to the absorber in the case of CPVT collector because of the lower thermal conductivity of the TE modules. This results in a higher outlet fluid temperature in the CPVT compared to the CPVT-TE collector. Additionally, the CPVT-TE using 0.5% graphene/water nanofluid, gives higher outlet fluid temperature compared to the CPVT-TE using only water as the cooling fluid. The reason for this is an enhancement in the convective heat transfer between the wall tube and the fluid by adding graphene nanoparticles compared to the base fluid (water).

Fig. 10



Variation of outlet fluid temperature for different considered system for cloudy day under London climatic conditions.

Fig. 11

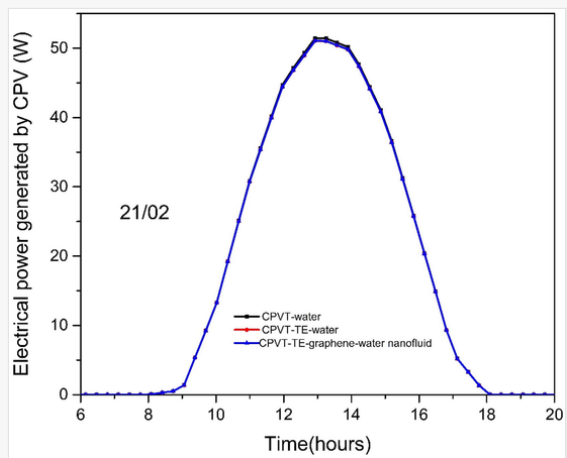


Variation of outlet fluid temperature for different considered system for sunny day under London climatic conditions.

4.2 Electrical power generated by CPV

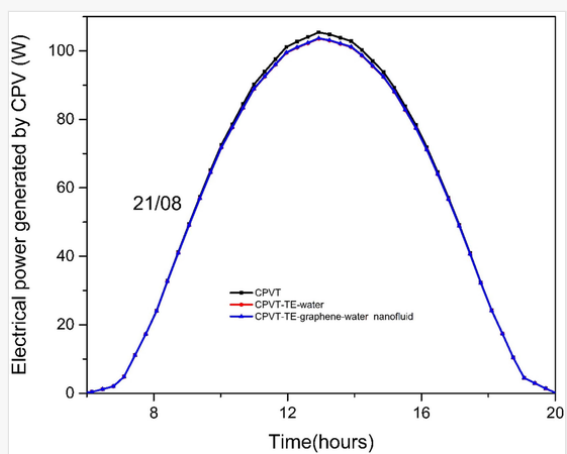
Figs. 12 and 13 show that the CPV in the CPVT collector generates the highest electrical power compared to CPV in CPVT-TE water collector and CPVT in CPVT-TE using 0.5% graphene/water nanofluid. For representative cold day (21/02) under London climatic conditions, the maximum power generated by the CPV in conventional CPVT was 51.91 W, while the maximum power generated by the CPV in CPVT-TE using water and using 0.5% graphene/water nanofluid were 51.5 W and 51.53 W, respectively. For representative summer day (21/08) under London climatic conditions, the maximum power generated by CPV in conventional CPVT was 105.58 W, while the maximum power generated by CPV in CPVT-TE using water and using 0.5% graphene/water were 103.72 W and 103.83 W, respectively. [Fig. 14.](#)

Fig. 12



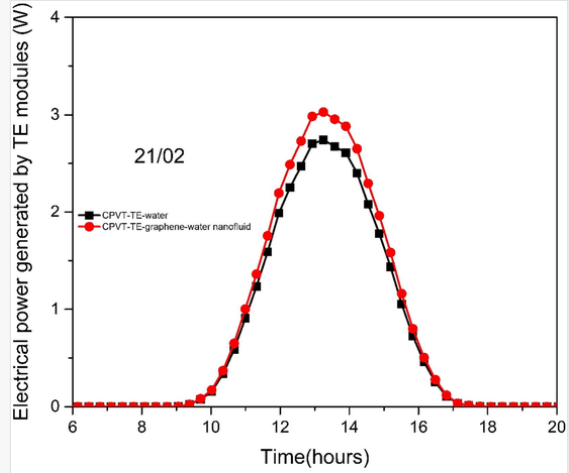
Variation of electrical power generated by CPV for different considered system for cloudy day under London climatic conditions.

Fig. 13



Variation of electrical power generated by CPV for different considered system for sunny day under London climatic conditions.

Fig. 14

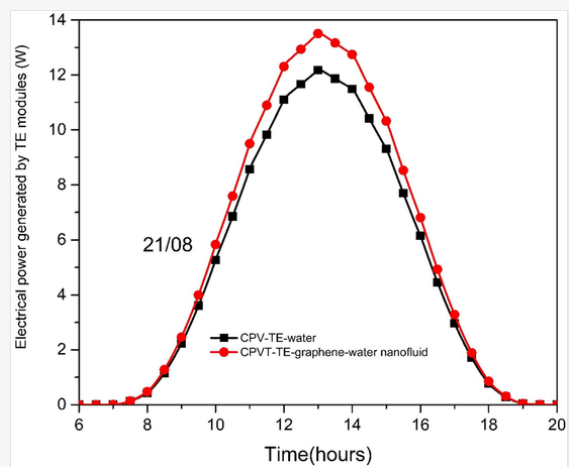


Variation of electrical power generated by thermoelectric modules for different considered system for cloudy day under London climatic conditions.

4.3 Electrical power generated by thermoelectric modules

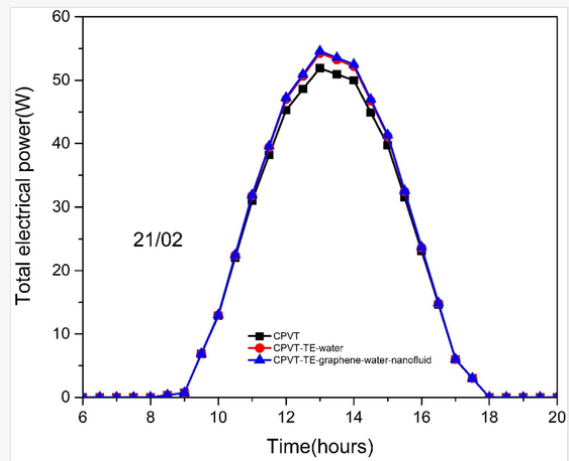
As shown in [Figs. 15](#) and [16](#), the CPVT-TE with 0.5% graphene/water nanofluid provides the highest electrical power generated by TE modules collector compared to the CPVT-TE using water a cooling fluid. For a chosen cold day (21/02) in London region, the maximum electrical power generated by TE modules in the CPVT-TE with 0.5% graphene/water nanofluid was 3.05 W, while the maximum electrical power generated by TE modules in the CPVT-TE using water was 2.76 W. On the other hand, for a chosen sunny day (21/08) in London region, the maximum electrical power generated by TE modules in the CPVT-TE with 0.5% graphene/water nanofluid was 13.52 W, while the maximum electrical power generated by TE modules in the CPVT-TE using water was 12.18 W.

Fig. 15



Variation of electrical power generated by thermoelectric modules for different considered system for sunny day under London climatic conditions.

Fig. 16

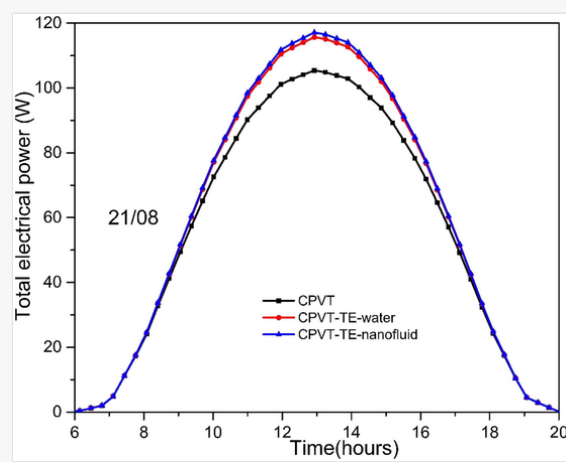


Variation of total electrical power generated for different considered system for cloudy day under London climatic conditions.

4.4 Total electrical power generated

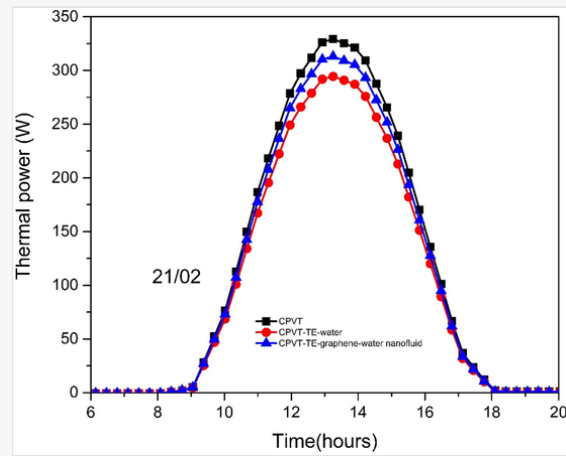
As shown in [Figs. 17](#) and [18](#), the CPVT-TE with 0.5% graphene/water nanofluid provides the highest electrical power compared to the CPVT-TE using water as cooling fluid, and the CPVT collector. For a chosen cold day (21/02) in London region, the maximum total electrical power generated by the CPVT-TE with 0.5% graphene/water nanofluid was 54.58 W, while the maximum total electrical power generated by the CPVT-TE using water and the conventional CPVT were 54.26 W and 51.91 W, respectively. On the other hand, for a chosen sunny day (21/08) in London region, the maximum total electrical power generated by the CPVT-TE with 0.5% graphene/water nanofluid was 117.35 W, while the maximum total electrical power generated by the CPVT-TE using water and the conventional CPVT were 115.90 W, and 105.58 W, respectively.

Fig. 17



Variation of total electrical power generated for different considered system for sunny day under London climatic conditions.

Fig. 18

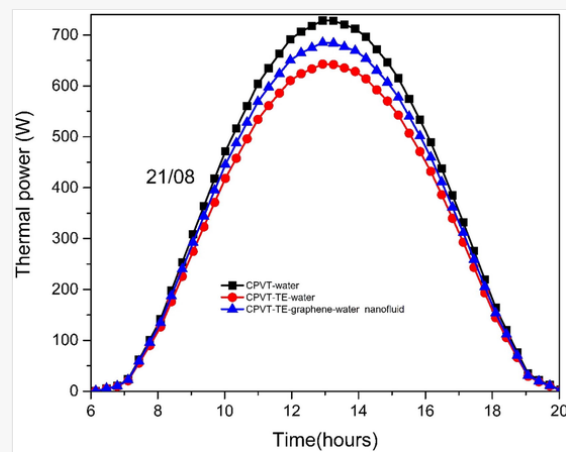


Variation of thermal power for different considered system for cloudy day under London climatic conditions.

4.5 Thermal power generated

As shown in Figs. 18 and 19, the CPVT collector produces the highest thermal power compared to the CPVT-TE collectors, either with water or with 0.5% graphene/water nanofluid. For a chosen cold day (21/02) in London region, the maximum thermal power provided by the CPVT collector was 330.6 W, while the maximum thermal power provided by the CPVT-TE collector using water and using 0.5% graphene/water nanofluid were 295.79 W to 314.52 W, respectively. On the other hand, for a chosen sunny day (21/08) in London region, the maximum thermal power provided by the CPVT collector was 731.48 W, while the maximum thermal power provided by the CPVT-TE collector using water and using 0.5% graphene/water nanofluid were 645.47 W to 687.57 W, respectively.

Fig. 19

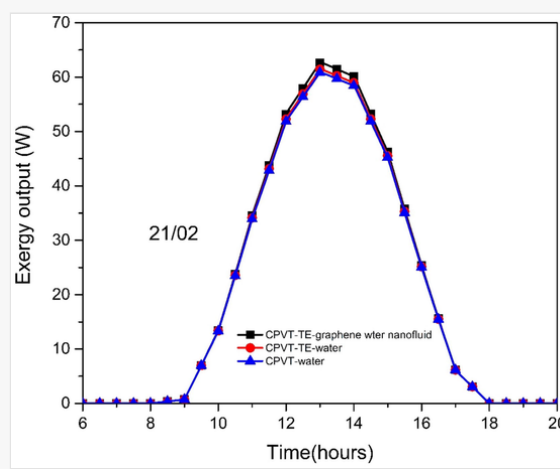


Variation of thermal power for different considered system for sunny day under London climatic conditions.

4.6 Exergy power outputs

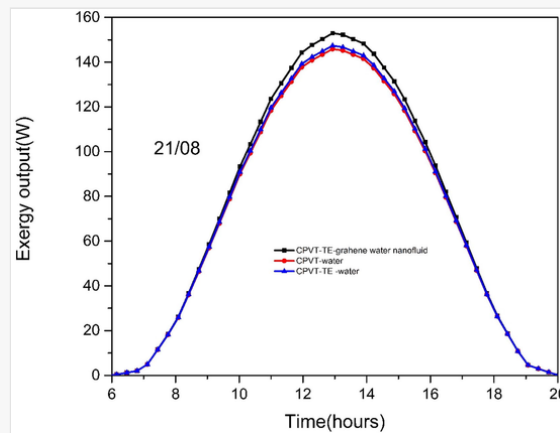
As shown in Figs. 20 and 21, the CPVT-TE with 0.5% graphene/water nanofluid collector produces the highest total exergy compared to the CPVT-TE with water and conventional CPVT collector. For a chosen cold day (21/02) in London region, the maximum total exergy power output provided by the CPVT-TE with 0.5% graphene/water nanofluid collector was 62.68 W, while the maximum total exergy power output provided by the CPVT-TE with water and conventional CPVT collector were 61.44 W, and 60.86 W, respectively. On the other hand, for a chosen sunny day (21/08) in London region, the maximum total exergy power output provided by the CPVT-TE with 0.5% graphene/water nanofluid collector was 153.54 W, while the maximum total exergy power output provided by the CPVT-TE with water and conventional CPVT collector were 147.38 W, and 146.38 W, respectively.

Fig. 20



Variation of exergy outputs for different considered system for cloudy day under London climatic conditions.

Fig. 21



Variation of exergy outputs for different considered systems for sunny day under London climatic conditions.

4.7 Overall summary

Tables 4–5 present a detailed comparison between the conventional CPVT, CPVT-TE with water and CPVT-TE with 0.5% graphene/water nanofluid from the CPV, outlet cooling temperatures variations, energy (electrical power generated by the CPV and by the TE modules, thermal power provided) and exergy viewpoints under London climatic conditions.

Table 4

i The table layout displayed in this section is not how it will appear in the final version. The representation below is solely purposed for providing corrections to the table. To preview the actual presentation of the table, please view the Proof.

Major findings for cloudy day under London climatic conditions.

	CPVT (baseline)	CPVT-TE water	CPVT-TE nanofluid	Major findings
CPV temperature	4.23 °C to 30.32 °C	4.64 °C to 33.87 °C	4.64 °C to 33.52 °C	For the cold day. An increase in the maximum CPV temperatures of the CPVT-TE with 0.5% graphene/water nanofluid, and water CPVT-TE collectors compared to CPVT collector is 10.611.71% and 10.5511.71% , respectively.
Outlet cooling temperature	4.6 °C to 16.29 °C	4.6 °C to 15.46 °C	4.6 °C to 15.91 °C	For the cold day. An reduction in the maximum outlet cooling temperature temperatures of the CPVT-TE with 0.5% graphene/water nanofluid, and water CPVT-TE collectors compared to CPVT collector is 2.152.33% and 4.945.09% , respectively.
Electrical power generated by CPV	51.91 W	51.5 W 0.78%	51.53 W 0.7339%	For the cold day. An reduction in the maximum Electrical powers generated by CPV in the CPVT-TE with 0.5% graphene/water nanofluid, and water CPVT-TE collectors compared to CPVT collector is 0.73% and 0.79%, respectively.
Electrical power generated TE		2.76 W	3.05 W	For the cold day. An improvement in the maximum Electrical power generated TE in the CPVT-TE with 0.5% graphene/water nanofluid, and collector compared to water CPVT-TE is 11.5910.51% .
Thermal power generated	330.60 W	295.79 W	314.52 W	For the cold day. An reduction in the maximum thermal powers provided by the CPVT-TE with 0.5% graphene/water nanofluid, and water CPVT-TE collectors compared to CPVT collector is 4.876% and 10.53% , respectively.
Total electrical	51.91 W	54.26 W	54.58 W	For the cold day. An improvement in the maximum total electrical power generated by the CPVT-TE with 0.5% graphene/water nanofluid, and water CPVT-TE collectors compared to CPVT collector is 5.14% and 4.528% , respectively.
Total exergy	60.86 W	61.44 W	62.68 W	For the cold day. An improvement in the maximum total exergy power generated by the CPVT-TE with 0.5% graphene/water nanofluid, and water CPVT-TE collectors compared to CPVT collector is 3.292.99% and 0.95% , respectively.

Table 5

i The table layout displayed in this section is not how it will appear in the final version. The representation below is solely purposed for providing corrections to the table. To preview the actual presentation of the table, please view the Proof.

Major findings for sunny day under London climatic conditions.

	CPVT	CPVT-TE water	CPVT-TE nanofluid	Major findings
CPV temperature	16.5 °C to 70.85 °C	16.6 °C to 77.96 °C	16.6 °C to 77.29 °C	For the sunny day. An increase in the maximum CPV temperatures of the CPVT-TE with 0.5% graphene/water nanofluid, and water CPVT-TE collectors compared to CPVT collector is 8.99% and 10.03% , respectively.
Outlet cooling temperature	16.6 °C to 39.8 °C	16.6 °C to 37.76 °C	16.6 °C to 38.76 °C	For the sunny day. An reduction in the maximum outlet cooling temperature temperatures of the CPVT-TE with 0.5% graphene/water nanofluid, and water CPVT-TE collectors compared to CPVT collector is 2.61% and 5.12%, respectively.
Electrical power generated by CPV	105.58 W	103.72 W	103.83 W	For the sunny day. An reduction in the maximum Electrical powers generated by CPV in the CPVT-TE with 0.5% graphene/water nanofluid, and water CPVT-TE collectors compared to CPVT collector is 1.66% and 1.76%, respectively.
Electrical power generated TE		12.18 W	13.52 W	For the sunny day. An improvement in the maximum Electrical power generated TE in the CPVT-TE with 0.5% graphene/water nanofluid, and collector compared to water CPVT-TE is 11%.
Thermal power generated	731.48 W	645.47 W	687.57 W	For the sunny day. An reduction in the maximum thermal powers provided by the CPVT-TE with 0.5% graphene/water nanofluid, and water CPVT-TE collectors compared to CPVT collector is 6% and 11.76%, respectively.
Total electrical	105.58 W	115.9 W	117.35 W	For the sunny day. An improvement in the maximum total electrical power generated by the CPVT-TE with 0.5% graphene/water nanofluid, and water CPVT-TE collectors compared to CPVT collector is 11.15% and 9.78%, respectively.
Total exergy	146.4 W	147.4 W	153.54 W	For the sunny day. An improvement in the maximum total exergy power generated by the CPVT-TE with 0.5% graphene/water nanofluid, and water CPVT-TE collectors compared to CPVT collector is 4.88% and 0.68%, respectively.

5 Conclusion

A detailed comparative study on a CPVT- TE with 0.5% graphene/water nanofluid, CPVT- TE with water and conventional CPVT collector was presented in this research. A transient study using the finite volume method is presented, and computation is performed for all the considered solar systems for a typical sunny day and cloudy day under London climatic conditions. The numerical model is applied to study the performance of the systems in terms of temperature variation, thermal and electrical energy and the total of exergy for the different considered systems. The main outcomes from this study are:

- The total electrical power produced by the CPVT-TE with 0.5% graphene/water nanofluid and CPVT-TE compared to CPVT collector is respectively 11.15% and 9.78% for the summer day, while, that for the winter day is 5.14% and 4.52%, respectively.
- The reductions in the thermal power provided by the CPVT-TE with 0.5% graphene/water nanofluid and CPVT-TE compared to CPVT collector are 6% and 11.76%, for the summer day, while, that for the winter day are 10.53% and 4.87%, respectively.
- The total exergies generated by 0.5% graphene/water nanofluid CPVT-TE and water CPVT-TE collectors increased by 4.88% and 0.68% respectively, for the summer day, while that for the winter day are 3.25% and 0.95% respectively, in comparison with the conventional CPVT system.

In the future, more work is required to investigate the energy, exergy, entropy and environmental assessments of the CPVT-TE with nanofluid phase change material (NPCM).

Q6 Unedited reference

[12].


Declaration of Competing Interest

The authors declare that they have no known competing financial interests or personal relationships that could have appeared to influence the work reported in this paper.

Acknowledgements

The authors would like to thank Sharjah Electricity and Water Authority (SEWA), the Sustainable Energy Development Research Group, and the Research Institute for Science and Engineering at the University of Sharjah for the financial support (postdoctoral position). The authors thank the Sustainable Energy Development Research Group, Sharjah Electricity and Water Authority (SEWA), and the Research Institute for Science and Engineering at the University of Sharjah for the financial support (postdoctoral position) at the University of Sharjah. Some of the authors benefits of the support of the French Investments for Future Program (ref. ANR-18-EURE-0016 - Solar Academy).

References

 The corrections made in this section will be reviewed and approved by a journal production editor. The newly added/removed references and its citations will be reordered and rearranged by the production team.

- [1] Liu H-B, Meng J-HH, Wang X-DD, Chen W-HH. A new design of solar thermoelectric generator with combination of segmented materials and asymmetrical legs. *Energy Convers Manag* 2018;175:11–20. doi:10.1016/j.enconman.2018.08.095.
- [2] Sampaio P.G.V., González M.O.A., de Vasconcelos R.M., dos Santos M.A.T., de Toledo J.C., Pereira J.P.P. Photovoltaic technologies: Mapping from patent analysis. *Renew Sustain Energy Rev* 2018;93:215–224. doi:10.1016/j.rser.2018.05.033.
- [3] Shittu S., Li G., Zhao X., Ma X. Review of thermoelectric geometry and structure optimization for performance enhancement. *Appl Energy* 2020;268:115075. doi:10.1016/j.apenergy.2020.115075.
- [4] Kabir E., Kumar P., Kumar S., Adelodun A.A., Kim K.H. Solar energy: Potential and future prospects. *Renew Sustain Energy Rev* 2018;82:894–900. doi:10.1016/j.rser.2017.09.094.
- [5] Sagani A., Mihelis J., Dedoussis V. Techno-economic analysis and life-cycle environmental impacts of small-scale building-integrated PV systems in Greece. *Energy Build* 2017;139:277–290. doi:10.1016/j.enbuild.2017.01.022.

- [6] Shittu S., Li G., Zhao X., Zhou J., Ma X. Experimental study and exergy analysis of photovoltaic-thermoelectric with flat plate micro-channel heat pipe. *Energy Convers Manag* 2020;207:112515. doi:10.1016/j.enconman.2020.112515.
- [7] Shittu S., Li G., Zhao X., Ma X. Series of detail comparison and optimization of thermoelectric element geometry considering the PV effect. *Renew Energy* 2019;130:930–942. doi:10.1016/j.renene.2018.07.002.
- [8] Rejeb O., Dhaou H., Jemni A. Parameters effect analysis of a photovoltaic thermal collector: Case study for climatic conditions of Monastir. Tunisia. *Energy Convers Manag* 2015;89:409–419. doi:10.1016/j.enconman.2014.10.018.
- [9] Rejeb O., Ghenai C., Jomaa M.H., Bettayeb M. Statistical study of a solar nanofluid photovoltaic thermal collector performance using response surface methodology. *Case Stud Thermal Eng* 2020;21:100721.
- [10] Rejeb O, Ghenai C, Jemni A, Bettayeb M. Performance Assessment of a Solar Photovoltaic Thermal Heat Pipe Collector under Hot Climate: A Case Study. 2019 *Adv Sci Eng Technol Int Conf ASET 2019* 2019:1–5. 10.1109/ICASET.2019.8714307.
- [11] Makki A., Omer S., Sabir H. Advancements in hybrid photovoltaic systems for enhanced solar cells performance. *Renew Sustain Energy Rev* 2015;41:658–684. doi:10.1016/j.rser.2014.08.069.
- [12] Shittu S., Li G., Akhlaghi Y.G., Ma X., Zhao X., Ayodele E. [Advancements in thermoelectric generators for enhanced hybrid photovoltaic system performance](#). *Renew Sustain Energy Rev* 2019;109:24–54. doi:10.1016/j.rser.2019.04.023.
- [13] Rejeb O., Gaillard L., Giroux-Julien S., Ghenai C., Jemni A., Bettayeb M., et al. Novel solar PV/Thermal collector design for the enhancement of thermal and electrical performances. *Renew Energy* 2020;146:610–627. doi:10.1016/j.renene.2019.06.158.
- [14] Huen P., Daoud W.A. Advances in hybrid solar photovoltaic and thermoelectric generators. *Renew Sustain Energy Rev* 2017;72:1295–1302. doi:10.1016/j.rser.2016.10.042.
- [15] Shittu S., Li G., Zhao X., Ma X., Akhlaghi Y.G., Ayodele E. Optimized high performance thermoelectric generator with combined segmented and asymmetrical legs under pulsed heat input power. *J Power Sources* 2019;428:53–66. doi:10.1016/j.jpowsour.2019.04.099.
- [16] Shittu S., Li G., Xuan Q., Xiao X., Zhao X., Ma X. Transient and non-uniform heat flux effect on solar thermoelectric generator with phase change material. *Appl Therm Eng* 2020;173:115206. doi:10.1016/j.applthermaleng.2020.115206.
- [17] Rejeb O., Shittu S., Ghenai C., Li G., Zhao X., Bettayeb M. Optimization and performance analysis of a solar concentrated photovoltaic-thermoelectric (CPV-TE) hybrid system. *Renew Energy* 2020;152:1342–1353.
- [18] Yin E., Li Q., Xuan Y. Feasibility analysis of a concentrating photovoltaic-thermoelectric-thermal cogeneration. *Appl Energy* 2019;560–573.
- [19] Shittu S., Li G., Zhao X., Ma X., Akhlaghi Y.G., Ayodele E. High performance and thermal stress analysis of a segmented annular thermoelectric generator. *Energy Convers Manag* 2019;184:180–193. doi:10.1016/j.enconman.2019.01.064.
- [20] Shittu S., Li G., Zhao X., Ma X., Akhlaghi Y.G., Fan Y. Comprehensive study and optimization of concentrated photovoltaic-thermoelectric considering all contact resistances. *Energy Convers Manag* 2020;205:112422. doi:10.1016/j.enconman.2019.112422.
- [21] Shittu S., Li G., Xuan Q., Zhao X., Ma X., Cui Y. Electrical and mechanical analysis of a segmented solar thermoelectric generator under non-uniform heat flux. *Energy* 2020;199:117433. doi:10.1016/j.energy.2020.117433.
- [22] Li G., Shittu S., Diallo T.M.O., Yu M., Zhao X., Ji J. A review of solar photovoltaic-thermoelectric hybrid system for electricity generation. *Energy* 2018;158:41–58. doi:10.1016/j.energy.2018.06.021.
- [23] Li G., Zhou K., Song Z., Zhao X., Ji J. Inconsistent phenomenon of thermoelectric load resistance for photovoltaic-thermoelectric module. *Energy Convers Manag* 2018;161:155–161. doi:10.1016/j.enconman.2018.01.079.
- [24] Rezanian A., Rosendahl L.A. Feasibility and parametric evaluation of hybrid concentrated photovoltaic-thermoelectric system. *Appl Energy* 2017;187:380–389. doi:10.1016/j.apenergy.2016.11.064.
- [25] Lamba R., Kaushik S.C. Solar driven concentrated photovoltaic-thermoelectric hybrid system: Numerical analysis and optimization. *Energy Convers Manag* 2018;170:34–49. doi:10.1016/j.enconman.2018.05.048.
- [26] Mahmoudinezhad S., Rezanian A., Rosendahl L.A. Behavior of hybrid concentrated photovoltaic-thermoelectric generator under variable solar radiation. *Energy Convers Manag* 2018;164:443–452. doi:10.1016/j.enconman.2018.03.025.
- [27] Mahmoudinezhad S., Atouei S.A., Cotfas P.A., Cotfas D.T., Rosendahl L.A., Rezanian A. Experimental and numerical study on the transient behavior of multi-junction solar cell-thermoelectric generator hybrid system. *Energy Convers Manag* 2019;184:448–455. doi:10.1016/j.enconman.2019.01.081.
- [28] Shittu S., Li G., Tang X., Zhao X., Ma X., Badieli A. Analysis of thermoelectric geometry in a concentrated photovoltaic-thermoelectric under varying weather conditions. *Energy* 2020;202:117742. doi:10.1016/j.energy.2020.117742.
- [29] Li G., Diallo T.M.O., Akhlaghi Y.G., Shittu S., Zhao X., Ma X., et al. Simulation and experiment on thermal performance of a micro-channel heat pipe under different evaporator temperatures and tilt angles. *Energy* 2019;179:549–557. doi:10.1016/j.energy.2019.05.040.
- [30] Shittu S., Li G., Zhao X., Akhlaghi Y.G., Ma X., Yu M. Comparative study of a concentrated photovoltaic-thermoelectric system with and without flat plate heat pipe. *Energy Convers Manag* 2019;193:1–14. doi:10.1016/j.enconman.2019.04.055.
- [31] Li G., Shittu S., Zhou K., Zhao X., Ma X. Preliminary experiment on a novel photovoltaic-thermoelectric system in summer. *Energy* 2019;188:116041. doi:10.1016/j.energy.2019.116041.
- [32] Cui T., Xuan Y., Li Q. Design of a novel concentrating photovoltaic-thermoelectric system incorporated with phase change materials. *Energy Convers Manag* 2016;112:49–60. doi:10.1016/j.enconman.2016.01.008.
- [33] Motiei P., Yaghoubi M., GoshtasbiRad E. Transient simulation of a hybrid photovoltaic-thermoelectric system using a phase change material. *Sustain Energy Technol Assessments* 2019;34:200–213. doi:10.1016/j.seta.2019.05.004.

- [34] Darkwa J., Calautit J., Du D., Kokogianakis G. A numerical and experimental analysis of an integrated TEG-PCM power enhancement system for photovoltaic cells. *Appl Energy* 2019;248:688–701. doi:10.1016/j.apenergy.2019.04.147.
- [35] Yin E., Li Q., Xuan Y. Thermal resistance analysis and optimization of photovoltaic-thermoelectric hybrid system. *Energy Convers Manag* 2017;143:188–202. doi:10.1016/j.enconman.2017.04.004.
- [36] Yin E., Li Q., Xuan Y. One-day performance evaluation of photovoltaic-thermoelectric hybrid system. *Energy* 2018;143:337–346. doi:10.1016/j.energy.2017.11.011.
- [37] Yin E., Li Q., Xuan Y. Experimental optimization of operating conditions for concentrating photovoltaic-thermoelectric hybrid system. *J Power Sources* 2019;422:25–32. doi:10.1016/j.jpowsour.2019.03.034.
- [38] Zhang J., Xuan Y. Performance improvement of a photovoltaic – Thermoelectric hybrid system subjected to fluctuant solar radiation. *Renew Energy* 2017;113:1551–1558. doi:10.1016/j.renene.2017.07.003.
- [39] Wu Y.Y., Wu S.Y., Xiao L. Performance analysis of photovoltaic-thermoelectric hybrid system with and without glass cover. *Energy Convers Manag* 2015;93:151–159. doi:10.1016/j.enconman.2015.01.013.
- [40] Soltani S., Kasaeian A., Sarrafha H., Wen D. An experimental investigation of a hybrid photovoltaic/thermoelectric system with nanofluid application. *Sol Energy* 2017;155:1033–1043. doi:10.1016/j.solener.2017.06.069.
- [41] Lekbir A., Hassani S., Ab Ghani M.R., Gan C.K., Mekhilef S., Saidur R. Improved energy conversion performance of a novel design of concentrated photovoltaic system combined with thermoelectric generator with advance cooling system. *Energy Convers Manag* 2018;177:19–29. doi:10.1016/j.enconman.2018.09.053.
- [42] Soltani S., Kasaeian A., Lavajoo A., Loni R., Najafi G., Mahian O. Exergetic and enviromental assessment of a photovoltaic thermal-thermoelectric system using nanofluids: indoor experimental tests. *Energy Convers. Manag.* 2020;218:112907. doi:10.1016/j.enconman.2020.112907.
- [43] Rajae F., Rad M.A.V., Kasaeian A., Mahian O., Yan W.-M. Experimental analysis of a photovoltaic/thermoelectric generator using cobalt oxide nanofluid and phase change material heat sink. *Energy Convers Manag* 2020;212:112780.
- [44] Kolahan A., Maadi S.R., Kazemian A., Schenone C., Ma T. Semi-3D transient simulation of a nanofluid-base photovoltaic thermal system integrated with a thermoelectric generator. *Energy Convers. Manage.* 2020;220:113073.
- [45] Lekbir A., Hassani S., Mekhilef S., Saidur R., Ab Ghani M.R., Gan C.K. Energy performance investigation of nanofluid-based concentrated photovoltaic/thermal-thermoelectric generator hybrid system. *Int J Energy Res.* 2021;1–19. doi:10.1002/er.6436.
- [46] Alous S., Kayfeci M., Uysal A. Experimental investigations of using MWCNTs and graphene nanoplatelets water-based nanofluids as coolants in PVT systems. *Appl Therm Eng* 2019;162:114265.
- [47] Riahi A, Ben Haj Ali A, Fadhel A, Guizani A, Balghouthi M. Performance investigation of a concentrating photovoltaic thermal hybrid solar system combined with thermoelectric generators. *Energy Convers Manag* 2020;205:112377, 10.1016/j.enconman.2019.112377

Highlights

- A comparison between the CPVT only system and CPVT-TE collectors is conducted.
- A transient study using finite volume method is performed for the solar systems.
- The impact of adding a 0.5% graphene/water nanofluid in CPVT-TE is analyzed.
- Energy and exergy assessment under London climatic condition is performed.

Queries and Answers

Q1

Query: Your article is registered as a regular item and is being processed for inclusion in a regular issue of the journal. If this is NOT correct and your article belongs to a Special Issue/Collection please contact s.sultana@elsevier.com immediately prior to returning your corrections.

Answer: done

Q2

Query: Please confirm that the provided email 'oussama.r009@hotmail.fr' is the correct address for official communication, else provide an alternate e-mail address to replace the existing one, because private e-mail addresses should not be used in articles as the address for communication.

Answer: yes

Q3

Query: The author names have been tagged as given names and surnames (surnames are highlighted in teal color). Please confirm if they have been identified correctly.

Answer: done

Q4

Query: The country name has been inserted for the affiliation 'f'. Please check, and correct if necessary.

Answer: done

Q5

Query: Fig. 14 was not cited in the text. We have cited in their corresponding places. Please check our placement of citation.

Answer: done

Q6

Query: Uncited references: This section comprises references that occur in the reference list but not in the body of the text. Please cite each reference in the text or, alternatively, delete it.

Any reference not dealt with will be retained in this section.

Answer: done